POLITECNICO DI TORINO
Repository ISTITUZIONALE

Accordion-like metamaterials with tunable ultra-wide low-frequency band gaps

Original
Accordion-like metamaterials with tunable ultra-wide low-frequency band gaps / Krushynska, A. O.; Amendola, A.; Bosia, F.; Daraio, C.; Pugno, N. M.; Fraternali, F.. - In: NEW JOURNAL OF PHYSICS. - ISSN 1367-2630. - 20:7(2018), p. 073051. [10.1088/1367-2630/aad354]

Availability:
This version is available at: 11583/2773495 since: 2019-12-14T10:55:33Z

Publisher:
Institute of Physics Publishing

Published
DOI:10.1088/1367-2630/aad354

Terms of use:

This article is made available under terms and conditions as specified in the corresponding bibliographic description in the repository

Publisher copyright

(Article begins on next page)

06 May 2026

New Journal of Physics
The open access journal at the forefront of physics

Deutsche Physikalische Gesellschaft DPG IOP Institute of Physics

PAPER • OPEN ACCESS

Accordion-like metamaterials with tunable ultra-wide low-frequency band gaps

To cite this article: A O Krushynska *et al* 2018 *New J. Phys.* **20** 073051

View the article online for updates and enhancements.

This content was downloaded from IP address 93.37.52.57 on 31/07/2018 at 08:04

New Journal of Physics
The open access journal at the forefront of physics

Deutsche Physikalische Gesellschaft DPG
IOP Institute of Physics

Published in partnership with: Deutsche Physikalische Gesellschaft and the Institute of Physics

OPEN ACCESS

RECEIVED
5 April 2018

REVISED
9 July 2018

ACCEPTED FOR PUBLICATION
13 July 2018

PUBLISHED
31 July 2018

Original content from this work may be used under the terms of the Creative Commons Attribution 3.0 licence.

Any further distribution of this work must maintain attribution to the author(s) and the title of the work, journal citation and DOI.

PAPER

Accordion-like metamaterials with tunable ultra-wide low-frequency band gaps

A O Krushynska[1,7], A Amendola[2], F Bosia[3], C Daraio[4], N M Pugno[1,5,6] and F Fraternali[2]

[1] Laboratory of Bio-Inspired and Graphene Nanomechanics, Department of Civil, Environmental and Mechanical Engineering, University of Trento, Via Mesiano, 77, I-38123 Trento, Italy
[2] Department of Civil Engineering, University of Salerno, Via Giovanni Paolo II, 132, I-84084 Fisciano (SA), Italy
[3] Department of Physics and Nanostrucured Interfaces and Surfaces Centre, University of Turin, Via P. Guria, 1, I-10125 Turin, Italy
[4] Engineering and Applied Science, California Institute of Technology, Pasadena, CA 91125, United States of America
[5] School of Engineering and Materials Science, Queen Mary University of London, Mile End Road, London E1 4NS, United Kingdom
[6] Ket Labs, Edoardo Amaldi Foundation, Italian Space Agency, Via del Politecnico snc, Rome I-00133, Italy
[7] Author to whom any correspondence should be addressed.

E-mail: akrushynska@gmail.com, adaamendola1@unisa.it, fbosia@unito.it, daraio@caltech.edu, nicola.pugno@unitn.it and f.fraternali@unisa.it

Keywords: wave dynamics, elastic metamaterial, tensegrity structure, ultra-wide band gap, low-frequency range

Supplementary material for this article is available online

Abstract

Composite materials with engineered band gaps are promising solutions for wave control and vibration mitigation at various frequency scales. Despite recent advances in the design of phononic crystals and acoustic metamaterials, the generation of wide low-frequency band gaps in practically feasible configurations remains a challenge. Here, we present a class of lightweight metamaterials capable of strongly attenuating low-frequency elastic waves, and investigate this behavior by numerical simulations. For their realization, tensegrity prisms are alternated with solid discs in periodic arrangements that we call 'accordion-like' meta-structures. They are characterized by extremely wide band gaps and uniform wave attenuation at low frequencies that distinguish them from existing designs with limited performance at low-frequencies or excessively large sizes. To achieve these properties, the meta-structures exploit Bragg and local resonance mechanisms together with decoupling of translational and bending modes. This combination allows one to implement selective control of the pass and gap frequencies and to reduce the number of structural modes. We demonstrate that the meta-structural attenuation performance is insensitive to variations of geometric and material properties and can be tuned by varying the level of prestress in the tensegrity units. The developed design concept is an elegant solution that could be of use in impact protection, vibration mitigation, or noise control under strict weight limitations.

1. Introduction

Engineered composites capable of manipulating elastic waves in an unconventional way [1–3] are rapidly becoming attractive in multiple application areas, including seismic wave shielding [4, 5], sub-wavelength imaging [6], vibration abatement [7, 8], acoustic cloaking [9], sound control [10], etc. A distinguishing peculiarity of these materials, also known as meta-structures [11], is their ability to generate band gaps—frequency ranges with inhibited wave propagation. In phononic crystals, periodic patterning of constituents or material phases activates Bragg scattering [12] opening band gaps at wavelengths comparable with the spatial periodicity [7, 13]. Acoustic metamaterials exploit local resonances to induce low-frequency band gaps allowing the control of waves at much larger wavelengths than their microstructural scales [14–16]. The local resonance effect is induced by coated inclusions or pillars, increasing the total structural weight. In this case, wave attenuation is efficient only at the resonator eigenfrequencies and abruptly decreases away from them [5, 14, 17–19]. Therefore, broadband control of low-frequency waves using lightweight structures remains a challenge.

© 2018 The Author(s). Published by IOP Publishing Ltd on behalf of Deutsche Physikalische Gesellschaft

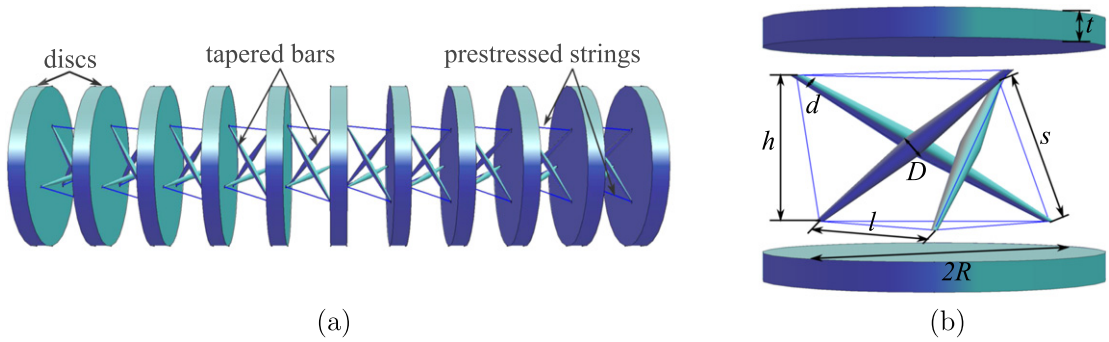

Figure 1. (a) Accordion-like meta-chain of circular discs interlayed by minimal tensegrity prisms, which are formed by tapered bars and prestressed strings; (b) structure and geometric parameters of a representative unit cell.

Band-gap widths can be enlarged by exploiting rainbow-trapping designs [5], topology optimization techniques [20, 21], or coupling the Bragg and local resonant mechanisms [18, 22]. Alternatively, the incorporation of slender elements with small values of effective stiffness can lower the Bragg scattering limit [20]. Simultaneous use of these strategies can provide promising results [11, 23].

Another constraint hindering practical applications of meta-structures is a fixed operating frequency range. Proposed tuning strategies include harnessing mechanical instabilities [15, 24], thermal radiation [25], piezoelectric effects [26] or magnetic nonlinearities [27], and incorporation of rotational elements [28]. These require a specific non-trivial material behavior or mobile constituent elements that entail expensive manufacturing processes and high exploitation costs. Therefore, metamaterial designs with easily adjustable functionalities remain to be developed.

In this work, we propose the use of tensegrity prisms as a new design strategy for realizing lightweight meta-structures with wide band gaps at low frequencies that can be tuned in a simple way by varying the level of prestress or tailoring the unit cell geometry. The developed designs with lattice-type units interlayered by solid discs resemble the structure of an accordion, leading us to adopt the term 'accordion-like' (figure 1(a)). The imposed continuity conditions between tensegrity units and solid discs ensure structural functionality and integrity. In addition, the absence of moving parts entails a simple fabrication process, e.g. using additive manufacturing techniques, making these structures cost-efficient and attractive for various applications.

We demonstrate that band gaps, originating from a combination of Bragg scattering in the slender bars and local resonances of the constituent elements, are particularly wide due to the decoupling of the bending and longitudinal modes in the peculiarly organized tensegrity prisms. The presence of several band-gap formation mechanisms ensures efficient wave attenuation using only a few meta-structural units. Finally, we show that the band gaps can further be merged, provided a minimum amount of structural damping is present, as is the case in all real materials.

The paper is organized as follows: section 2 describes the model and properties of the developed meta-structures. Section 3 discusses the structural dispersion and transmission characteristics, as well as the mechanisms of the band-gap formation and tunability. The main conclusions are given in section 4. Additional details are provided in three appendices.

2. Metamaterial model

Among the plethora of design possibilities for tensegrity structures [29], we choose the simplest regular minimal prism shown in figure 1(b). By periodically alternating it with circular discs, we create a one-dimensional meta-chain. A representative unit cell of the chain consists of the prism and two halves of the terminal discs.

The regular tensegrity prism of height h is composed of three inclined tapered bars connected by five prestressed strings. Two strings form horizontal equilateral triangles of side length l at the ends of the bars, which can rotate relative to each other by an arbitrary twist angle ϕ. Simple geometric considerations lead to the relation between the bar length b, the length of the three cross-strings s and the other parameters:

$$b = \sqrt{h^2 + \frac{4}{3}l^2 \sin^2\frac{\phi}{2}}, \qquad s = \sqrt{b^2 + \frac{\sqrt{3}}{2}l^2 \cos\left(\phi + \frac{\pi}{6}\right)}. \tag{1}$$

We assume continuous displacements at the prism-disc joints, implying that tapered bars and discs constitute a continuous chain made of a single-phase material. This assumption ensures structural robustness and allows us to eliminate the horizontal strings from further consideration.

The discs are identical with thickness $t = 2$ mm and radius $R = 10$ mm. We assume the cables to be made of 0.28 mm diameter PowerPro® Spectra fibers (Young's modulus $E_f = 5.48$ GPa and mass density $\rho_f = 793$ kg m^{-3}), which are among the strongest and lightest fibers available on the market, with particularly high specific strength and remarkable durability [30]. The material of the bars and the discs is assumed to be titanium alloy Ti6A14V (Young's modulus $E_t = 120$ GPa, Poisson's ratio $\nu_t = 0.33$, and mass density $\rho_t = 4450$ kg m^{-3}), which is widely employed in industrial applications, including additive manufacturing through electron beam melting (see [31] and references therein). The choice of materials is also dictated by the availability of experimental tests on the tensegrity structures of the same composition [32]. The central and end diameters of a bar are $D = 0.8$ mm and $d = 0.18$ mm, respectively. For non-prestressed strings, $p_0 = 0$, the prism height is $h_0 = 5.407$ mm and the triangle side is $l_0 = 8.7$ mm. The material volume fraction is 27%, corresponding to an effective unit-cell density $\rho_{\text{eff}} = 1216$ kg m^{-3}, evaluated as the sum of the material phase density multiplied by its volume fraction.

3. Elastic waves in tensegrity meta-chains

3.1. Dispersion analysis

Assuming linear elastic behavior of the constituents (see appendix A), we first analyze an equilibrium non-prestressed configuration of the meta-chain with $\phi = 5\pi/6$ and $p_0 = 0$ [31]. Finite-element simulations (see appendix B for details) reveal that the corresponding dispersion relation has six adjacent band gaps shown in figure 2(a). Their mid-gap frequencies are 10.02 kHz, 18.93 kHz, 32.10 kHz, 41.50 kHz, 51 kHz and 73.30 kHz, and the normalized gap width (the percentage ratio between the gap width and the mid-gap frequency) is 38.2%, 69.3%. 38.8%, 9.1%, 21.2%, and 46.3%, respectively.

To understand the mechanisms governing the wave dispersion, we consider the mode polarization, indicated by the color of the dispersion curves. Blue describes translational modes without bending deflections of the discs; red corresponds to pure bending modes. The degree of bending deflection b of the discs is evaluated as:

$$b = \frac{\int_A (|\omega_x|^2 + |\omega_y|^2)\,\mathrm{d}A}{\int_A (|\omega_x|^2 + |\omega_y|^2 + |\omega_z|^2)\,\mathrm{d}A} = \frac{\int_A (|\omega_{xk_z}|^2 + |\omega_{yk_z}|^2)\,\mathrm{d}A}{\int_A (|\omega_{xk_z}|^2 + |\omega_{yk_z}|^2 + |\omega_{zk_z}|^2)\,\mathrm{d}A}, \tag{2}$$

where $|\omega_x|^2 = \omega_x\bar{\omega}_x = \left(\frac{\partial u_z}{\partial y} - \frac{\partial u_y}{\partial z}\right)\left(\frac{\partial \bar{u}_z}{\partial y} - \frac{\partial \bar{u}_y}{\partial z}\right)$; $|\omega_y|^2 = \omega_y\bar{\omega}_y = \left(\frac{\partial u_x}{\partial z} - \frac{\partial u_z}{\partial x}\right)\left(\frac{\partial \bar{u}_x}{\partial z} - \frac{\partial \bar{u}_z}{\partial x}\right)$; $|\omega_z|^2 = \omega_z\bar{\omega}_z = \left(\frac{\partial u_y}{\partial x} - \frac{\partial u_x}{\partial y}\right)\left(\frac{\partial \bar{u}_y}{\partial x} - \frac{\partial \bar{u}_x}{\partial y}\right)$. Here, $A = \pi R^2 t$, and the superimposed bar indicates complex conjugation. The subscript k_z designates that component ω_i (with i denoting x, y or z) is evaluated for a fixed value of k_z at the Brillouin zone border $\Gamma - Z$. In figure 2(a), all the modes are of either pure translational or pure bending polarization, i.e., the two fundamental mode types are fully decoupled, which is not the case for most existing continuous and lattice-type meta-structures. This feature results in a comparatively small number of the dispersion curves (see, e.g., the dispersion relations in [11, 20, 23]), since the coupled modes are absent, which in turn enables the generation of multiple band gaps.

The two lowest translational modes (figures 2(b) and (c)) with parallel uniform axial motions of the discs are analogous to the fundamental translational mode in a one-dimensional mass-spring system [12]. The second of the modes (figure 2(c)) exists due to the continuity conditions between a prism and two discs and has maximum displacements at the joints. Note that translational motions are accompanied by small rotations of the discs in their planes, as alterations of the prism height are coupled to variations of the twist angle ϕ [31, 33]. Hence, it is more accurate to refer to these modes as 'translational-twisting'.

The mode forming the upper bound of the first band gap is governed by the bending displacements of the discs (figure 2(d)). The decrease of the displacements towards the center of the bars suggests that bending momenta are inefficiently transmitted through the tapered inclined bars, as in the case of extremal materials [34].

The modes at the edges of the higher-frequency band gaps exhibit either confined vibrations in the inclined bars (figures 2(e), (g) and (h)) or higher-order bending harmonics of the discs with the bars at rest (figures 2(f) and (i)). The corresponding flat dispersion bands in figure 2(a) have a close-to-zero group velocity typical for localized motions.

The decoupling of the translational-twisting and bending modes is attributed to the peculiarities of wave propagation through the inclined bars of a tapered geometry. Simulations show that when the bars are perpendicular to the discs (see appendix B, figure B1(b)), the lowest band gap disappears; the translational and bending modes become coupled, and the rotational components degenerate (see appendix B, figure B1(d)). If the end diameter of the inclined bars increases (i.e., tapering is reduced), the band-gap edges move to higher frequencies, the gap widths decrease, and the separation between adjacent band gaps increases (see appendix B, figure B2(a)). In this case, the modes are again coupled, as can be seen by the color change of dispersion bands (see supplementary video 1 available online at stacks.iop.org/NJP/20/073051/mmedia). However, even for

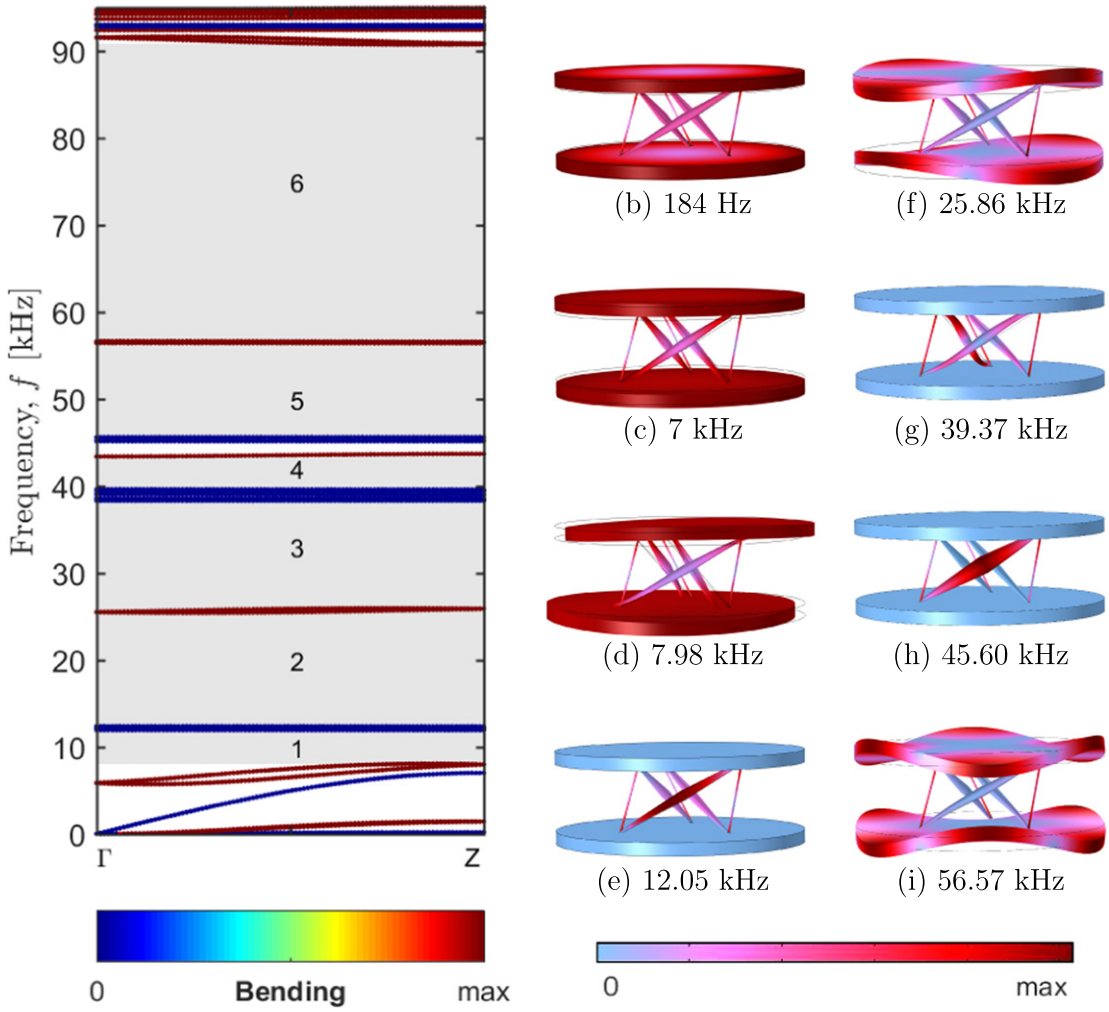

Figure 2. (a) Dispersion relation for an accordion-like meta-chain with discs of radius $R = 10$ mm and thickness $t = 2$ mm. Shaded regions denote frequency band gaps (numbered from 1 to 6). The color of the dispersion curves indicates the level of bending deflection of the discs evaluated using equation (2). Mode shapes are calculated at the Z point of the Brillouin zone. The color designates the distribution of the total displacements, $\sqrt{u_x^2 + u_y^2 + u_z^2}$, within the unit cell ranging from zero (metallic blue) to a maximum value (metallic red).

straight bars of a constant cross-section and for bars with thicker ends than the central diameter (figure B2(c)), the wave attenuation functionality is preserved (figure B2(a)), which distinguishes the proposed 'accordion-like' meta-structures from other designs with tapered bars, e.g. pentamode materials [34]. It should be also noted that the feature of the mode decoupling is preserved for three-dimensional accordion-like designs analyzed in appendix C.

An additional advantage of using tensegrity prisms is the reduction of the total structural weight. The comparison of data in figure 3, showing the band-gap widths of several optimized metamaterial designs as a function of their effective density, reveals that the accordion-like meta-structures have the smallest material filling fraction and the widest band-gap sizes at low frequencies. The reported data refer to three-dimensional or two-dimensional (in-plane waves) configurations of continuous (bold lines) or cellular (dashed lines) structures. The band-gap widths have been re-calculated for a unit cell size of 10 mm, based on the data provided in the original works [17–21, 35], for a uniform comparison.

3.2. Transmission through finite-size meta-chains

To evaluate the actual wave attenuation performance of the accordion-like configurations, we analyze wave transmission through a meta-chain of a finite size. Figure 4 shows the magnitude of total transmitted displacements $\sqrt{u_x^2 + u_y^2 + u_z^2}$ averaged upon three adjacent discs and normalized with respect to the applied excitation u_{z0}. The blue (solid), red (dotted) and black (dashed) curves correspond to displacements at distances of 3, 5, and 10 unit cells from the loaded end. The attenuation of waves passing through only 5 unit cells is uniform and largely exceeding three orders of magnitude even for localized pass bands. The

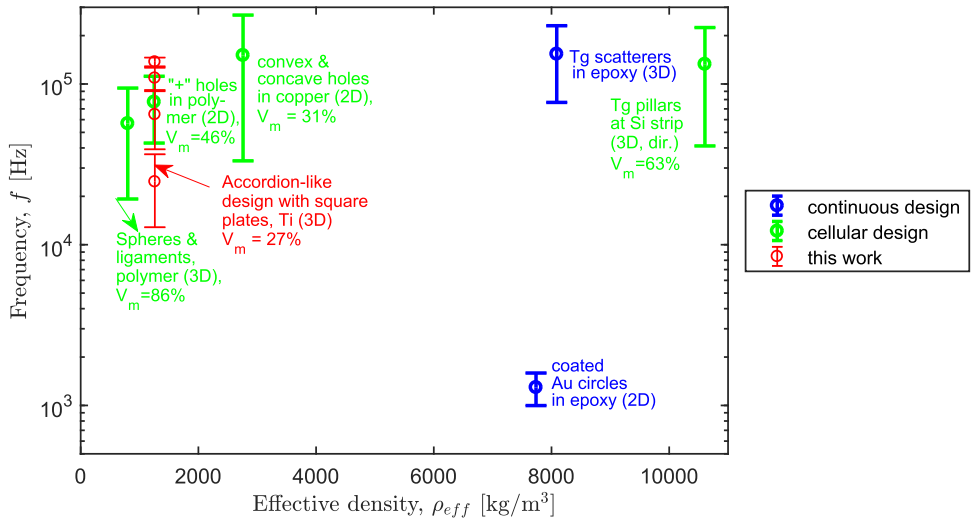

Figure 3. Band-gap widths for meta-structures with optimized low-frequency attenuation. The unit cell size is $h_{uc} = 10$ mm and the material volume fraction V_m are indicated for each structure. The initial data are taken from [17] for coated Au circles in epoxy; [21] for convex and concave holes in copper; [35] for cross-like holes in a polymer; [20] for polymeric spheres joined by ligaments; [19] for Tg scatterers in epoxy; [18] for Si strip with Tg pillars.

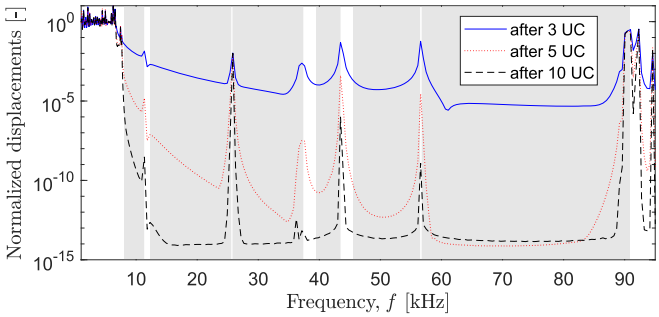

Figure 4. Normalized transmitted displacements $\sqrt{u_x^2 + u_y^2 + u_z^2}/u_{z0}$ versus frequency f for an accordion-like meta-chain (30 unit cells). The curves indicate the displacement values averaged on three adjacent discs at distances of 3, 5, or 10 units from the loaded end. The unit cell parameters are $R = 10$ mm, $t = 2$ mm for the discs, and $D = 0.8$ mm, $d = 0.18$ mm, $h = 5.407$ mm, $l = 8.7$ mm for the tensegrity prisms with non-prestressed strings.

translational-twisting modes characterized by intense motions in bars are more attenuated compared to bending modes. This occurs partly due to the applied structural damping in the bars (see appendix B for details), but also due to an inherent difficulty to excite isolated vibrations in the bars while keeping the discs motionless. Based on this argument and the data in figure 4, we conclude that the first two pairs of band gaps are merged into two wide band gaps with a gap width of 103.6% and 50.6%. An excellent agreement between the band gaps of an infinite meta-structure (figure 2(a)) and those for a finite-size chain confirms the accuracy of the numerical simulations.

3.3. Band-gap mechanism

To gain a deeper insight into the origin of the band-gap formation mechanism, we estimate the Bragg mid-gap frequency $f^B_{\text{mid}} = c_p/(2h_{uc})$ deriving from the structural periodicity, where c_p is the phase velocity of waves propagating in the medium. For cellular-type structures with slender elements, the phase velocity depends on effective medium parameters, such as the effective stiffness modulus and the effective mass density. In our case, the values of c_p can be extracted directly from the dispersion relation in figure 2(a) as the ratio $2\pi f/k$ in the vicinity of the Γ point for each mode type [11]. For the translational-twisting modes, the frequency f^B_{mid} is located at the intersection between a tangent to the second mode (green solid line in appendix B, figure B1(c)) and the vertical line $k_z = Z$. This frequency falls within the first band gap, indicating that Bragg scattering governs the gap formation mechanism. An additional argument supporting this conclusion is the uniform level of wave attenuation at the inhibited frequencies (figure 4), typical for Bragg band gaps [22, 36].

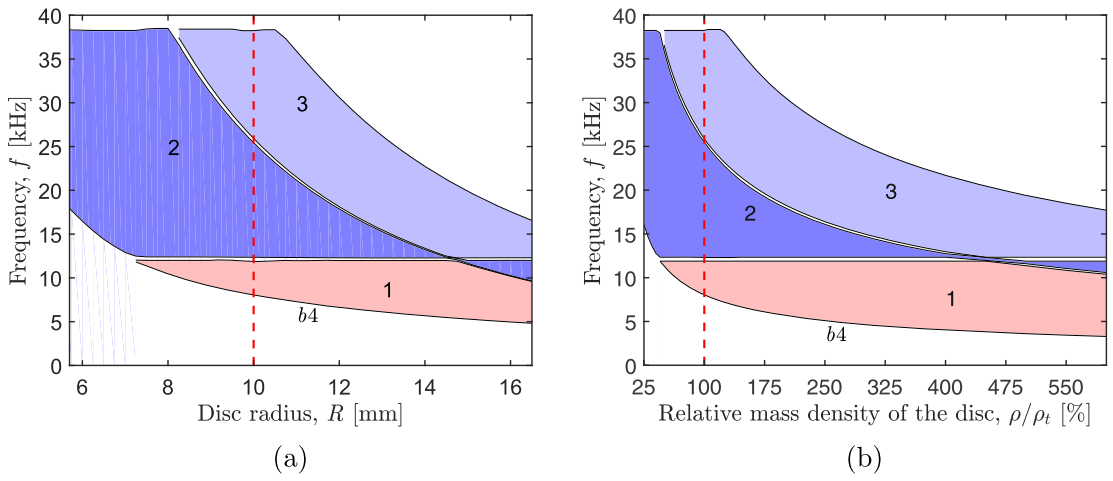

Figure 5. Frequencies of the three lowest band gaps (numbered from 1 to 3) versus the radius (a) or the mass density (b) of a disc normalized to the mass density of titanium ρ_t. The red dashed line refers to the dispersion relation shown in figure 2(a). The notation b4 indicates the fourth bending mode that is the lower bound of the first band gap.

On the other hand, the flattening of the dispersion bands at the band-gap edges (figure 2(a)) and localized character of the corresponding mode shapes (figures 2(e)–(i)) clearly point to the presence of local resonant effects. The involvement of local resonances is also demonstrated in appendix B (figure B2(a)), where the band-gap edges are flat for varying material filling fraction of the bars [17].

Therefore, the resulting complete band gaps in the accordion-like meta-structures originate from a superposition of the Bragg scattering and local resonances. This provides multiple possibilities for varying the gap width and tuning the pass bands by manipulating frequencies of selected modes linked to the structural geometry.

3.4. Band-gap tunability

Variations of geometric parameters of the unit cells result in different dispersion characteristics of a meta-chain. For example, by altering the bar geometry one can shift the band gaps to different frequencies or modify the band widths, as shown in section 3.1. Similarly, one can alter the disc sizes. Figure 5(a) shows the dependence between the disc radius R and the frequencies of the three lowest band gaps. The corresponding dispersion relations are presented in supplementary video 2. Results show that the increase of R can shift the band gaps to about half their previous frequencies. Note that the related variations of the effective mass density and the material volume fraction are small and range from $\rho_{\text{eff}} = 1250\ \text{kg m}^{-3}$ and $V_m = 28\%$ to $\rho_{\text{eff}} = 1206\ \text{kg m}^{-3}$ and $V_m = 25\%$ for the analyzed geometries. For discs of a larger radius, the shift to lower frequencies is accompanied by the excitation of localized and bending modes that reduce the gap widths.

The variations of the material mass density (normalized to the mass density of titanium ρ_t) provide similar results, as shown in figure 5(b) (the related dispersion curves can be found in supplementary video 3). These data can also be considered as representative of inhomogeneous meta-structures with the discs made from a different material. To facilitate the comparison with the homogeneous case, the disc geometry is fixed.

The flat edges of the second and third band gaps in figure 5 confirm the involvement of the local resonance effect in the band gap formation [17], while the monotonic decrease of the lower edge of the first band gap indicates the presence of other effects. These data agree well with the conclusions relative to the simultaneous presence of several band-gap mechanisms discussed in section 3.3.

Another possibility to tune the band gaps is to vary the prestress level in the incorporated cross-strings. The prestressed state follows from the action of a set of self-equilibrated internal forces or applied external tensile loading, and can be usefully characterized through the prestrain level $p_0 = (s - s_0)/s_0$, where s_0 is an initial non-prestrained length of a cross-string. The prestress alters the prism height, modifies its geometry and mechanical response, as shown in table 2 of [37]. For our structures, the prism height h varies from $5.407\ \text{mm}$ for $p_0 = 0$ to $5.97\ \text{mm}$ for $p_0 = 0.1$. The analyzed range of the applied prestrain is restricted to experimentally realistic values [38]. Larger prestrain levels may result in variations of the axial stiffness of the tensegrity prisms and thus require the incorporation of nonlinear constitutive equations (see appendix A for details).

The variation of the prestrain level naturally results in modifications of the band-gap frequencies, as shown in figure 6. Here, the frequency $f^* = fh_{uc}/c_p$ is normalized with respect to effective phase velocity c_p in the

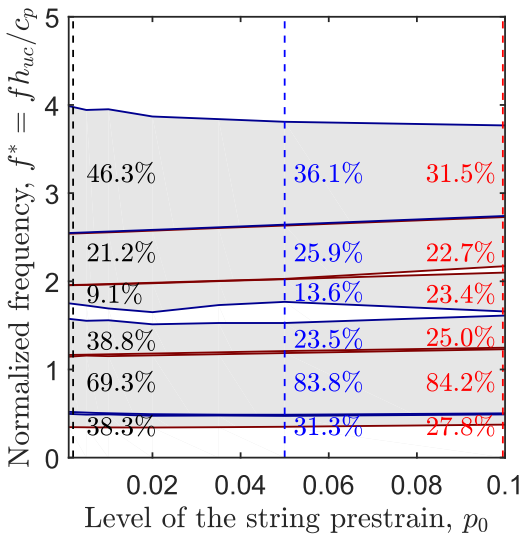

Figure 6. Band-gap frequencies (shaded regions) versus the level of the string prestrain p_0 in the cross-strings for an accordion-like meta-chain. The percentage indicates the normalized gap width for the prestrain level denoted by the dashed curves (the black curve at $p_0 = 0$, the blue curve at $p_0 = 0.05$, and the red curve at $p_0 = 0.1$). The unit cell parameters are the same as in figure 2. The blue and red band-gap bounds indicate, respectively, the absence and the maximum amount of bending deflections of the discs evaluated according to equation (2).

disc-bar material. This means that the tunability of the gap width is less dependent on the material characteristics of the solids, and governed by the elasticity of the strings. The numbers in figure 6 indicate the normalized gap width at different levels of prestrain. They reveal that the percentage changes in the band-gap frequencies can reach 15%, which can be of interest for many practical applications.

Possible approaches to introduce prestress include either the application of external mechanical forces *in situ* or the utilization of micro-stereolitography setups for manufacturing the strings. The latter use materials that strongly contract, when dehydrated, and thus create internal prestrain (see [37] and the references therein). The exploitation of materials with different values of thermal expansion coefficients also opens a way to control the level of prestrain by varying the ambient temperature.

4. Conclusion

In summary, we have developed metamaterial designs supporting multiple low-frequency band gaps with uniform wave attenuation performance. With a material filling fraction of 27%, they are the lightest practically feasible configurations reported to date (to the best of our knowledge). A significant weight reduction is achieved by periodically alternating solid elements with tensegrity prisms in 'accordion-like' configurations. This peculiar structure enables to decouple translational from bending modes, while the continuity conditions between the lattice and solid elements improve the wave attenuation functionality and contribute to structural integrity and robustness. Thus, the proposed metamaterials can easily be fabricated by means of additive manufacturing techniques from a wide range of materials at comparatively low costs.

We have demonstrated that the band gaps originate from a superposition of Bragg scattering and local resonances of slender elements combined with the decoupling of longitudinal and bending modes. These features ensure strong wave attenuation at the band-gap frequencies by means of a limited number of unit cells and provide ample freedom in tuning pass and gap bands by selective modifications of the unit-cell geometry. The geometry-based nature of wave attenuation mechanisms makes them independent of a specific material, and thus, broadband low-frequency band gaps can be induced in 'accordion-like' configurations made of a wide spectrum of materials. Additional tunability of the band-gap frequencies can be achieved exploiting variations of the prestress level in the strings incorporated in the tensegrity units. Our numerical results reveal that the gap widths are maintained with respect to variations in the material or geometric parameters, whereas optimal band-gap merger is obtained for tapered designs of the inclined bars.

Our study demonstrates the promising nature of accordion-like designs for broadband control of low-frequency elastic waves. In the presence of a small level of structural damping, which is present in all real

materials, the gap width exceeds 100%, making these meta-structures especially attractive for various applications, including vibration mitigation or impact and shock wave protection.

Finally, the developed designs can be seen as modifications of 'extremal' materials [39], which inhibit the propagation of shear waves only, if the diameter of tapered ends is small [34]. We have shown that our meta-structures are not subject to this restriction and can generate low-frequency band gaps even if the end diameter of inclined bars is larger than the central one. Further interesting possibilities can be envisioned for future extensions to recently proposed 'rank 2' and 'rank 3' walled structures [40].

Acknowledgments

AA, FB, NMP, and FF acknowledge financial support from the Italian Ministry of Education, University and Research (MIUR) under the 'Departments of Excellence' grant L.232/2016. NMP is supported by the European Commission under the Graphene Flagship Core 2 grant No. 785219 (WP14 'Composites') and with FB by the FET Proactive 'Neurofibres' grant No. 732344. FB also acknowledges the support by Progetto d'Ateneo/Fondazione San Paolo 'Metapp', n. CSTO160004.

Compliance with Ethical Standards

The authors declare that they have no conflict of interest.

Appendix A. Linearized response of accordion-like meta-structures

The mechanical response of tensegrity prisms with bars, which are allowed to rotate freely, is governed solely by the level of prestress in the cross-cables [38, 41]. This behavior is described by a nonlinear stress–strain relation due to geometric effects emerging from large values of the twist angle ϕ [31, 33]. For small oscillations of the prisms around their initial positions, as in the case of small-amplitude waves, this relation can be linearized, and the prisms act as linear springs. At low frequencies, the dynamics of a meta-chain, in which the prisms alternate solid discs in frictionless contact, is thus analogous to that of a one-dimensional linear spring-mass system, as discussed in [37].

On the contrary, in the accordion-like meta-structures with continuity conditions between the prisms and discs, the axial stiffness of the prism k_h also depends on tangential stiffness of the bars, and is thus non-zero in the absence of prestress. The k_h can be estimated by means of finite-element simulations taking into account geometric nonlinearities (Comsol Multiphysics 5.2). For this purpose, we consider an equilibrium configuration of the unit cell with the twist angle $\phi = 5\pi/6$ in the absence of prestretch $p_0 = 0$ (figure B1(a)). A tensile force is distributed at at the top surface of the upper disc in a unit cell, while the bottom disc is clamped. The estimated dependence of the stiffness k_h on the force F is given in table A1. Note that up to displacements of the order of 10^{-6} m, the axial stiffness is nearly constant. This justifies the assumption that the accordion-like unit cell exhibits a linear response to a small amplitude excitation. Therefore, the dynamic response of the designed metamaterials can be described by a linear constitutive relation that allows us to use the standard Bloch-wave analysis procedure.

Table A1. Relation between the static loading F and induced axial displacement u_z in the accordion-like unit cell. The axial stiffness is evaluated as $k_h = F/u_z$.

F (N)	u_z (m)	k_h (N m^{-1})
3.18×10^{-5}	$7.820\,9 \times 10^{-9}$	4061
3.18×10^{-4}	$7.820\,8 \times 10^{-8}$	4061
3.18×10^{-3}	$7.820\,8 \times 10^{-7}$	4061
1.59×10^{-2}	$3.906\,8 \times 10^{-6}$	4065

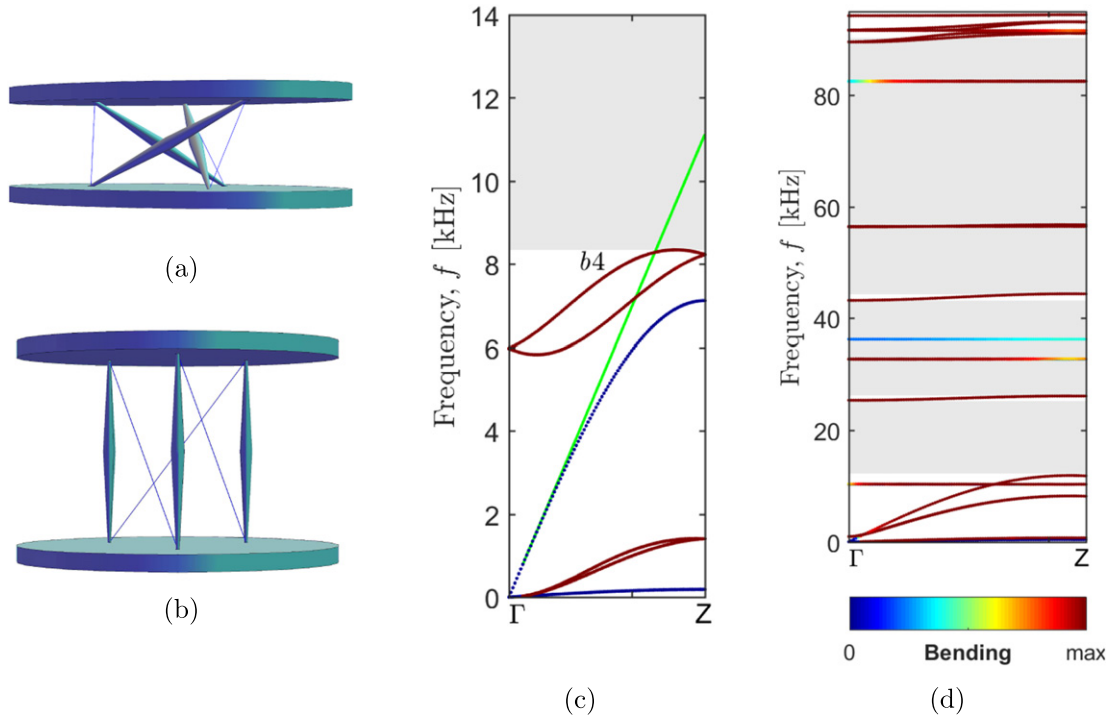

Figure B1. Unit cells of an accordion-like meta-chain with the twist angle of the tapered bars $\phi = 5\pi/6$ (a) and $\phi = 0$ (b). (c) The low-frequency part of the dispersion relation for the unit cell with $\phi = 5\pi/6$. The Bragg mid-gap frequency for translational-twisting modes is located at the intersection of the green line with the vertical line $k_z = Z$. (d) The dispersion relation for the metamaterial unit cell with $\phi = 0$. In (c), (d) the band gaps are highlighted by shaded regions, and the color of the dispersion curves indicates the level of bending deflections of the discs evaluated by means of equation (2).

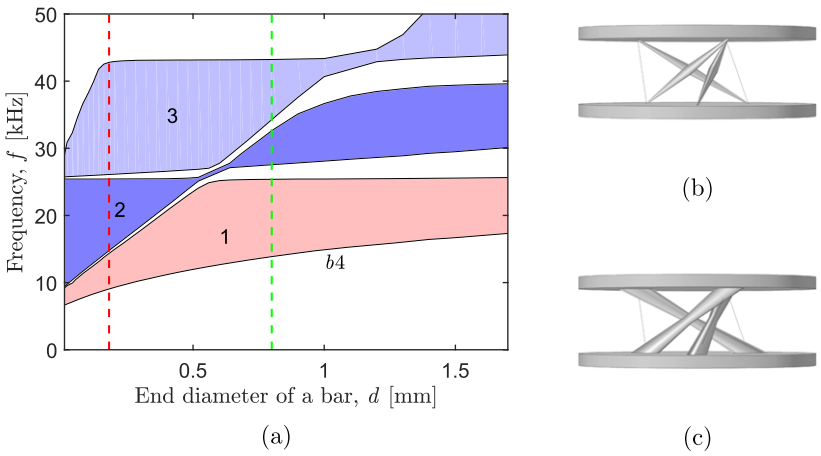

Figure B2. (a) Frequencies of the three lowest band gaps (numbered from 1 to 3) versus the end diameter of a bar in the tensegrity prism. The green and red dashed lines indicate the bars of a uniform cross section ($d = D$) and a reference configuration with dispersion relation shown in figures 2(a). (b), (c) The unit cells with the end diameters of a bar (b) $d = 0.1$ mm and (c) $d = 1.7$ mm.

Appendix B. Numerical models and methods

The wave dynamics of the accordion-like metamaterials is studied numerically by means of the finite-element method using Comsol Multiphysics 5.2. The dispersion relations are evaluated for a single unit cell with the Floquet–Bloch conditions at central cross-sections of the discs. The lateral faces of the discs are free of stresses. The related eigenfrequency problem is solved for positive real values of wavenumber k_z at the border of the irreducible Brillouin zone Γ–Z.

Wave transmission is estimated in the frequency domain for a finite-size meta-chain composed of 30 unit cells. One end of the chain is excited with an axial displacement of amplitude $u_{z0} = 0.1\ \mu$m applied uniformly to the disc surface. Another end is attached to a perfectly matched layer (of 5 unit cell size) to minimize undesired wave reflections. We eliminate unrealistically large displacements at resonant frequencies by introducing a vibration loss factor in the material of the bars. The loss factor η takes into account inherent structural damping in a dynamically loaded material and enters the stress–strain relationship as $\boldsymbol{\sigma} = D(1 + j\eta)\boldsymbol{\epsilon}$. We choose $\eta = 0.001$ Pa s that corresponds to the minimum value of losses in titanium alloys, as assessed experimentally [42].

Figures B1(a) and (b) show unit cells of the accordion-like meta-structure analyzed in the main text and with the bars perpendicular to the discs ($\phi = 0$), respectively. The corresponding dispersion relations are given in figures B1(c) and (d). The color of the dispersion bands indicates the level of bending deflections ranging from 0 to a maximum value. Figure B1(c) presents a low-frequency part of the relation shown in figure 2(a) with the label 'b4' describing the fourth bending modes. The frequency at the intersection of the green line with the vertical line at the edge of the Brilloiun zone $k_z = Z$ approximately equals the Bragg mid-frequency for the translational-twisting modes in the tapered bars.

Figure B2(a) presents the frequencies of the three band gaps versus the end diameter d of the bars. Green and red dashed lines refer to the bars of a uniform cross section ($d = D$) and the case analyzed in the main text with $d = 0.18$ mm (figure 2(a)), respectively. The unit cell geometries with the smallest and largest analyzed values of d are depicted in figures B2(b) and (c).

Appendix C. Three-dimensional accordion-like metamaterials

To analyze the dynamics of three-dimensional accordion-like structures, we replace the circular discs by square elements (figure C1(a)). The thickness of an element, $t = 2$ mm, is the same as for the discs. The lateral size of the square is $b = 17.72$ mm, so that the circular disc in a meta-chain analyzed in the main text (figure 2(a)) and the square element in the three-dimensional meta-structure have equal masses.

A three-dimensional model is obtained by periodic replications of the unit cells along three mutually perpendicular directions. Such a design restricts the excitation of bending modes in the low-frequency range, which dominate in the meta-chain with stress-free lateral faces.

The dispersion analysis is performed numerically by applying the Floquet–Bloch boundary conditions at the three pairs of the unit-cell faces. The absence of translational and rotational symmetries in the unit cell design requires to analyze the values of wave vector $\mathbf{k} = \{\mathrm{k}_x, \mathrm{k}_y, k_z\}$ within the irreducible Brillouin zone depicted by a parallelepiped in figure C1(b). To simplify the consideration, we analyze only specified directions and planes within the Brillouin zone highlighted in figure C1(b).

We first examine the direction Γ–Z with $k_x = 0$ and $k_y = 0$ describing a wave propagation perpendicular to the central planes of the square elements. Figure C1(c) shows the dispersion relation with multiple adjacent band gaps at low frequencies, similar to that for a meta-chain with circular discs (figure 2(a)). The distinctive feature is a smaller number of dispersion curves, most of which belong to the translational-twisting modes. The bending modes appear only at higher frequencies, when a quarter of the wavelength of shear bulk waves approximately equals the unit-cell size, i.e., $f = c_s/(4h_{uc}) \approx 45$ kHz with c_s denoting the shear wave velocity in titanium. Therefore, they originate due to the Bragg scattering at the lateral boundaries of the square elements.

The mode shapes of the two lowest translational-twisting modes (figures C1(d) and (e)) resemble those for the meta-chain with circular discs (figures 2(b) and (c)). The highest of the two forms a lower bound of the first band gap, while the upper band-gap bound is a flat curve describing a localized mode with vibrating bars (figure C1(f)). The first band gap is generated at almost the same frequencies as in the meta-chain (see figure 2(a)).

The dispersion relations for several cross-sections of the Brillouin zone (figure C1(b)) and their projections are shown in figure C2. Their inspection reveals the conservation of most of the band gaps in the case of oblique waves (figures C2(a)–(d)), which makes the designed accordion-like meta-structures particularly attractive for practical applications. The worst situation occurs if waves propagate in the plane of the square elements (figures C2(e) and (f)), since the attenuation mechanisms based on interactions between the solid and tensegrity parts become inefficient. Nevertheless, even in this case, the lowest band gap is preserved.

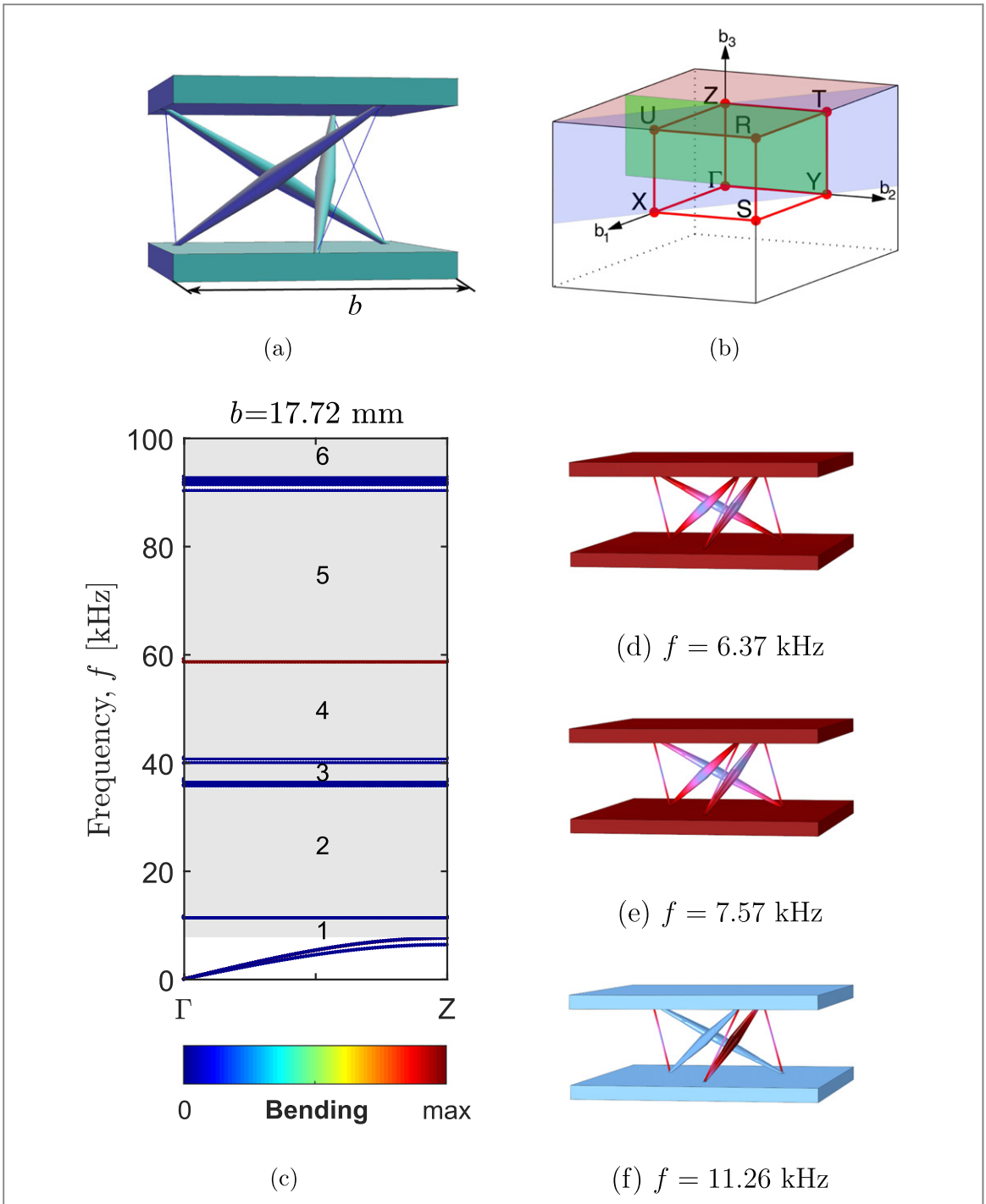

Figure C1. (a) Unit cell of an accordion-like meta-structure with square terminal elements; (b) the corresponding Brillouin zone in the k-space with the irreducible part highlighted by red edges. (c) The dispersion relation for waves propagating along $\Gamma-Z$ direction in the three-dimensional accordion-like meta-structure. Band gaps numbered from 1 to 6 are highlighted by shaded regions. (d)–(f) Selected mode shapes at point Z.

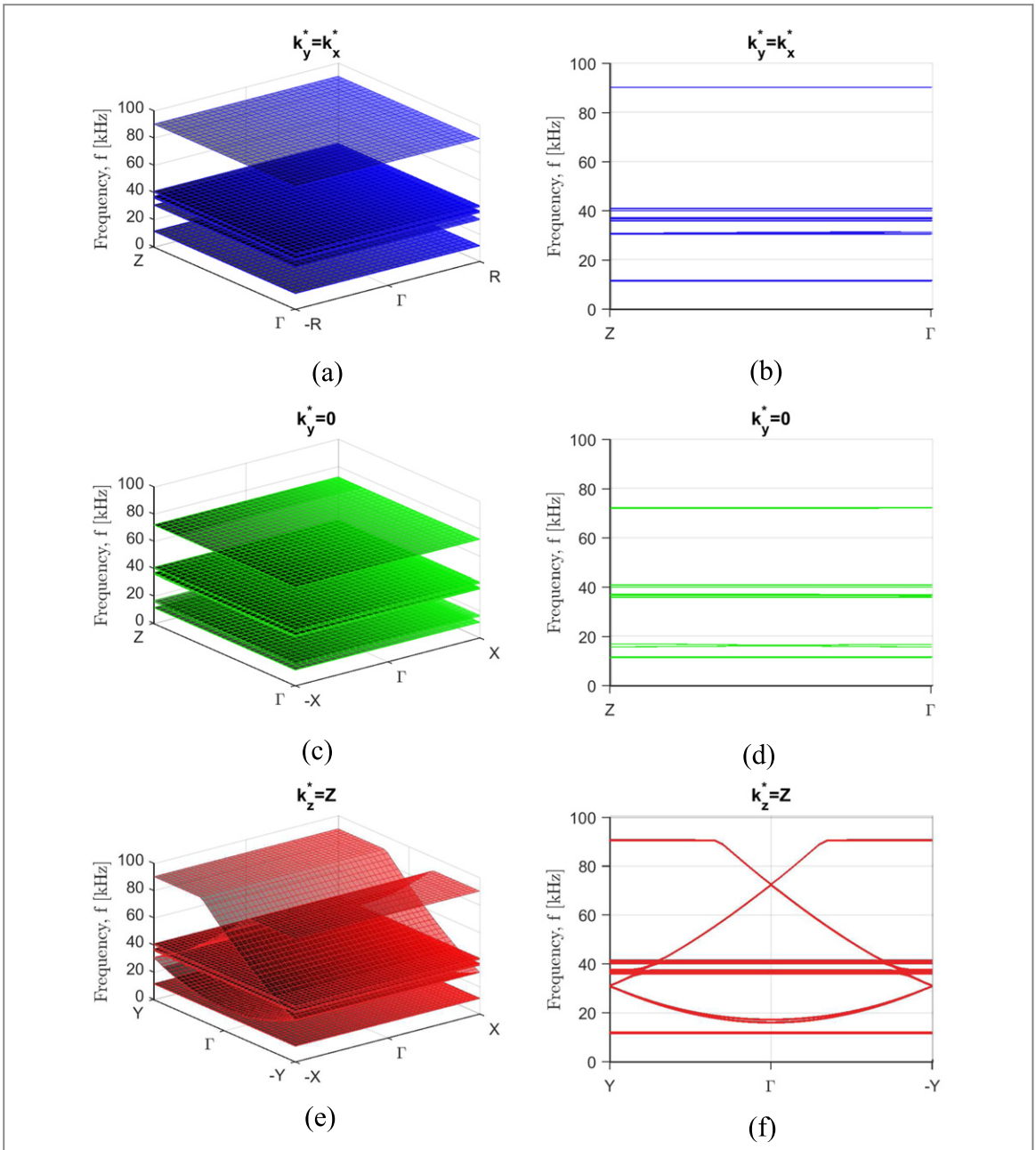

Figure C2. Dispersion surfaces for an accordion-like metamaterial with square terminal elements (figure C1(a)). The graphs in (b), (d), (f) show the two-dimensional projections of the surfaces in graphs (a), (c), (e). The surfaces are calculated for values of the wave vector $\mathbf{k} = \{k_x, k_y, k_z\}$ indicated by corresponding colors in figure C1(b).

ORCID iDs

A O Krushynska https://orcid.org/0000-0003-3259-2592
A Amendola https://orcid.org/0000-0002-2562-881X
F Bosia https://orcid.org/0000-0002-2886-4519
C Daraio https://orcid.org/0000-0001-5296-4440
N M Pugno https://orcid.org/0000-0003-2136-2396
F Fraternali https://orcid.org/0000-0002-7549-6405

References

[1] Craster R V and Gueanneau S 2013 *Acoustic Metamaterials: Negative Refraction, Imaging, Lensing and Cloaking* (Berlin: Springer)
[2] Maier S A (ed) 2017 *World Scientific Handbook of Metamaterials and Plasmonics. Vol 2: Elastic, Acoustic, and Seismic Metamaterials* (Singapore: World Scientific)

[3] Cummer S A, Christensen J and Alu A 2016 Controlling sound with acoustic metamaterials *Nat. Rev. Mater.* **1** 16001
[4] Brûlé S, Javelaud E H, Enoch S and Guenneau S 2014 Experiments on seismic metamaterials: molding surface waves *Phys. Rev. Lett.* **112** 133901
[5] Colombi A, Colquitt D, Roux P, Guenneau S and Craster R V 2016 A seismic metamaterial: the resonant metawedge *Sci. Rep.* **6** 27717
[6] Zhang S, Yin L and Fang N 2009 Focusing ultrasound with an acoustic metamaterial network *Phys. Rev. Lett.* **102** 194301
[7] Sánchez-Pérez J V, Caballero D, Mártinez-Sala R, Rubio C, Sánchez-Dehesa J, Meseguer F, Llinares J and Gálvez F 1998 Sound attenuation by a two-dimensional array of rigid cylinders *Phys. Rev. Lett.* **80** 5325
[8] Ho K M, Cheng C K, Yang Z, Zhang X X and Sheng P 2003 Broadband locally resonant sonic shields *Appl. Phys. Lett.* **83** 5566
[9] Fahrat M, Enoch S, Guenneau S and Movchan A B 2008 Broadband cylindrical acoustic cloak for linear surface waves in a fluid *Phys. Rev. Lett.* **101** 134501
[10] Krushynska A O, Bosia F, Miniaci M and Pugno N M 2017 Spider web-structured labyrinthine acoustic metamaterials for low-frequency sound control *New J. Phys.* **19** 105001
[11] Matlack K H, Bauhofer A, Krödel S, Palermo A and Daraio C 2016 Composite 3D-printed metastructures for low-frequency and broadband vibration absorption *Proc. Natl Acad. Sci.* **113** 8386–90
[12] Brillouin L 1946 *Wave Propagation in Periodic Structures* (New York: McGraw-Hill)
[13] Martínez-Sala R, Sancho J, Sánchez J V, Gómez V, Llinares J and Meseguer F 1995 Sound attenuation by sculpture *Nature* **378** 241
[14] Liu Z, Zhang X, Mao Y, Zhu Y Y, Yang Z, Chan C T and Sheng P 2000 Locally resonant sonic materials *Science* **289** 1734–6
[15] Wang P, Casadei F, Shan S, Weaver J C and Bertoldi K 2014 Harnessing buckling to design tunable locally resonant acoustic metamaterials *Phys. Rev. Lett.* **113** 0140301
[16] Beli D, Arruda J R F and Ruzzene M 2018 Wave propagation in elastic metamaterial beams and plates with interconnected resonators *Int J. Solids Struct.* **139–140** 105–20
[17] Krushynska A O, Kouznetsova V G and Geers M G D 2014 Towards optimal design of locally resonant acoustic metamaterials *J. Mech. Phys. Solids* **71** 179–96
[18] Coffy E, Lavergne T, Addouche M, Euphrasie S, Vairac P and Khelif A 2015 Ultra-wide acoustic band gaps in pillar-based phononic crystal strips *J. Appl. Phys.* **118** 214902
[19] Lu Y, Yang Y, Guest J K and Srivastava A 2017 3-D phononic crystals with ultrawide band gaps *Sci. Rep.* **7** 43407
[20] D'Alessandro L, Belloni E, Ardito R, Corigliano A and Braghin F 2016 Modeling and experimental verification of an ultra-wide bandgap in 3D phononic crystals *Appl. Phys. Lett.* **109** 221907
[21] Jiang S, Hu H and Laude V 2017 Ultra-wide band gap in two-dimensional phononic crystal with combined convex and concave holes *Phys. Status Solidi RRL* **12** 1700317
[22] Yuan B, Humphrey V F, Wen J and Wen X 2013 On the coupling of resonance and Bragg scattering effects in three-dimensional locally resonant sonic materials *Ultrasonics* **53** 1332–43
[23] Krushynska A O, Miniaci M, Bosia F and Pugno N M 2017 Coupling local resonance with Bragg band gaps in single-phase mechanical metamaterials *Ext. Mech. Lett.* **12** 30–6
[24] Babaee S, Viard N, Wang P, Fang N X and Bertoldi K 2016 Harnessing deformation to switch on and off the propagation of sound *Adv. Mater.* **28** 1631–5
[25] Walker E, Reyes D, Rojas M M, Krokhin A, Wang Z and Neogi A 2014 Tunable ultrasonic phononic crystal controlled by infrared radiation *Appl. Phys. Lett.* **105** 143503
[26] Kherraz N, Haumesser L, Levassort F, Benard P and Morvan B 2018 Hybridization bandgap induced by an electrical resonance in piezoelectric metamaterial plates *J. Appl. Phys.* **123** 094901
[27] Bilal O R, Foehr A and Daraio C 2017 Reprogrammable phononic metasurfaces *Adv. Mater.* **29** 1700628
[28] Li X-F, Ni X, Feng L, Lu M-H, He C and Chen Y-F 2011 Tunable unidirectional sound propagation through a sonic-crystal-based acoustic diode *Phys. Rev. Lett.* **106** 084301
[29] Skelton R E and de Oliveira M C 2010 *Tensegrity Systems* (Berlin: Springer)
[30] Lee S M (ed) 1989 *Reference Book for Composites Technology* vol 1 (Lancaster, PA: Technomic Publishing)
[31] Fraternali F, Carpentieri G, Amendola A, Skelton R E and Nesterenko V F 2014 Multiscale tunability of solitary wave dynamics in tensegrity metamaterials *Appl. Phys. Lett.* **105** 201903
[32] Amendola A, Hernández-Nava E, Goodall R, Todd I, Skelton R E and Fraternali F 2015 On the additive manufacturing, post-tensioning and testing of bi-material tensegrity structures *Compos. Struct.* **131** 66–71
[33] Davini C, Micheletti A and Podio-Guidugli P 2016 On the impulsive dynamics of T3 tensegrity chains *Meccanica* **51** 2763–76
[34] Martin A, Kadic M, Schittny R, Bückmann T and Wegener M 2012 Phonon band structures of three-dimensional pentamode metamaterials *Phys. Rev.* B **86** 155116
[35] Wang Y-F, Wang Y-S and Su X-X 2011 Large band-gaps of two-dimensional phononic crystals with cross-like holes *J. Appl. Phys.* **110** 113520
[36] Laude V, Achaoui Y, Benchabane S and Khelif A 2009 Evanescent Bloch waves and the complex band structure of phononic crystals *Phys. Rev.* B **80** 092301
[37] Amendola A, Krushynska A O, Daraio C, Pugno N M and Fraternali F 2018 Tuning frequency band gaps of tensegrity metamaterials with local and global prestress *Int. J. Solids Struct.* (https://doi.org/10.1016/j.ijsolstr.2018.07.002)
[38] Amendola A, Fraternali F, Carpentieri G, de Oliveira M and Skelton R E 2014 Experimental investigation of the softening-stiffening response of tensegrity prisms under compressive loading *Compos. Struct.* **117** 234–43
[39] Milton G W and Cherkaev A V 1995 Which elasticity tensors are realizable? *J. Eng. Mater. Technol.* **117** 483–93
[40] Milton G W, Briane M and Harutyunyan D 2017 On the possible effective elasticity tensors of 2-dimensional and 3-dimensional printed materials *Math. Mech. Complex Syst.* **5** 41–94
[41] Oppenheim I and Williams W 2000 Geometric effects in an elastic tensegrity structure *J. Elast.* **59** 51–65
[42] Lee D-G, Lee S and Lee Y 2008 Effect of precipitates on damping capacity and mechanical properties of Ti–6Al–4V alloy *Mater. Sci. Eng.* A **486** 19–26